RSC Advances

PAPER

View Article Online
View Journal | View Issue

Cite this: *RSC Adv.*, 2023, **13**, 24918

Synthesis of niobium(IV) carbide nanoparticles *via* an alkali-molten-method at a spatially-limited surface of mesoporous carbon †

Keigo Tashiro, *[a] Shogo Kobayashi,[a] Hinako Inoue,[a] Akihide Yanagita, [a] Shuhei Shimoda[b] and Shigeo Satokawa*[a]

Received 16th May 2023
Accepted 15th August 2023

DOI: 10.1039/d3ra03254j

rsc.li/rsc-advances

One-pot synthesis of niobium carbabide (NbC) nanoparticles with *ca.* 30–50 nm was achieved *via* a rationally designed novel alkali-molten salt method using niobium oxide (Nb_2O_5), potassium carbonate (K_2CO_3), and mesoporous carbon (MPC). In this reaction, potassium niobate ($KNbO_3$) was produced as an intermediate and carbonization of $KNbO_3$ proceeds at a spatially limited external surface encompassed by the mesopores of MPC due to the repulsive characteristics of ionic $KNbO_3$ toward hydrophobic MPC, which affords the size-controlled NbC nanoparticles with a narrow particle distribution. The particle sizes tended to become smaller as the pore sizes of MPCs or the temperature on the calcination under the nitrogen stream decreased. Elemental reactions along the one-pot synthesis of NbC nanoparticles were clarified by X-ray spectroscopic, thermogravimetric, and mass spectrometric measurements.

Introduction

Catalytic reactions such as hydrogen production, methanol synthesis, Fischer–Tropsch synthesis, and reverse water gas shift reaction are essential to realizing carbon neutrality using sustainable energy production aiming to emit essentially no carbon dioxide.[1–5] In these catalytic processes, noble metals such as platinum have been widely used as active sites in catalysis. However, due to their scarcity, their use in sustainable energy production is currently not realistic. From the background, alternative materials of the noble metals are strongly desired.

Transition metal carbides (TMCs) are expected as alternatives to noble metals since TMCs possess high melting point, high corrosion resistance, and significant electronic and catalytic characteristics.[6–18] Among the many TMCs, niobium carbide (NbC) has attracted chemists because of its mechanical and chemical stability, and excellent electrochemical potential.[19] NbC was conventionally synthesized by calcination at high temperature after mixing niobium(v) oxide (Nb_2O_5) and carbon sources, affording adamant NbC with large particle sizes.[20] However, the growth of the particle size causes a decrease in the amount of active sites per weight.

Regarding this, the preparation of nano-sized NbC has been addressed by a lot of researchers to increase active sites per weight on the catalysis.[6,21–32] Recently, Tour and Zhao *et al.* synthesized NbC nanoparticles with *ca.* 20 nm of size *via* novel flash Joule heating in the reactor composed of capacitor banks, electrodes, quartz and a carbon source.[21] Takanabe and his co-workers succeeded in the synthesis of various TMCs including NbC nanoparticles with the size of <10 nm by a skillful strategy using ethanol solution of metal precursors and mesoporous graphitic carbon nitride (mpg-C_3N_4), in which the TMC nanoparticles were produced in the mesopores of mpg-C_3N_4.[22] As we can see in the pioneered study such as aforementioned literature, the key point on the preparation of size-controlled TMC nanoparticles is "reaction field". In other words, the size-controlled TMC nanoparticles are afforded resulting from precise design of the reaction field of a carbonization of metal species precursor.

Here, we reported a rationally designed new one-pot synthetic method of NbC nanoparticles with 30–50 nm by using Nb_2O_5, potassium carbonate (K_2CO_3), and hydrophobic mesoporous carbon (MPC). The key strategy of this method is utilizing a prohibition of capillary action (CA) of intermediated potassium niobate ($KNbO_3$) into the nano-sized pores of MPC due to significantly low affinity between them, resulting in the formation and growth of NbC particles at limited external surface encompassed by the pores as a reaction field (Fig. 1). Pore size of MPC had a direct relationship to area of the external surface unit, hence the size of resulting NbC nanoparticles was

[a]*Graduate School of Science and Technology, Seikei University, 3-3-1 Kichijoji, Kitamachi, Musashino-shi, Tokyo, 180-8633, Japan. E-mail: satokawa@st.seikei.ac.jp; keigo-tashiro@st.seikei.ac.jp*

[b]*Institute for Catalysis, Hokkaido University, Kita 21 Nishi 10, Kita-ku, Sapporo-shi, Hokkaido, 001-0021, Japan*

† Electronic supplementary information (ESI) available. See DOI: https://doi.org/10.1039/d3ra03254j

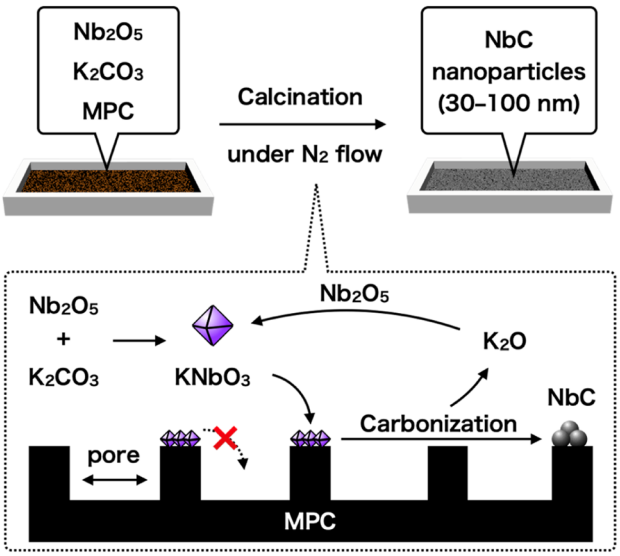

Fig. 1 Schematic representation of the alkali-molten method proposed in this study.

also changed by varying the pore size of MPC. Moreover, the nanoparticle sizes of the synthesized NbC gradually became smaller as the calcination temperature decreased, indicating a possibility of precise adjustment of particle sizes. Furthermore, we propose elemental reactions during the synthesis of NbC nanoparticles from Nb_2O_5.

Results and discussion

The NbC nanoparticles were synthesized from Nb_2O_5 and MPC possessing 150 nm of mean pore size (MPC-150) with K_2CO_3 under N_2 atmosphere. Fig. 2 displays X-ray diffraction (XRD) patterns of niobium species after calcination of the physical mixture of Nb_2O_5 and MPC with/without K_2CO_3 at 1150 °C under N_2 stream. In the case of the absence of K_2CO_3, NbC was formed accompanied by residual reduced niobium oxide species (NbO_2, $Nb_{12}O_{29}$) with the NbC yield of 31.8% estimated

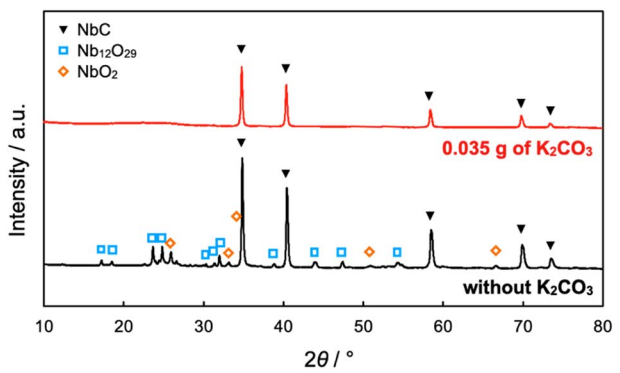

Fig. 2 XRD patterns of products after calcination of the mixture of Nb_2O_5 (0.1 g) and MPC-150 (0.1 g) with or without K_2CO_3 at 1150 °C for 10 h under N_2 stream atmosphere. The yield of NbC was estimated to be 31.8% on the absence of K_2CO_3.

by reference intensity ratio (RIR) method, while Nb_2O_5 was completely converted to NbC under the presence of K_2CO_3. This finding indicates that K_2CO_3 promoted the formation of NbC. To explore the impact of carbon sources on the synthesis of NbC nanoparticles, graphite was used instead of MPC. Although XRD measurements revealed that NbC could be produced regardless of carbon source, crystalline size (D) of NbC synthesized with graphite (D = 55 nm, Fig. S1†) was larger than that with MPC-150 (D = 32 nm). Moreover, transmission electron microscopic (TEM) images showed that NbC prepared with graphite tended to grow compared to NbC obtained by MPC-150 because the average particle sizes calculated by manual estimation of diameter of 200 of NbC particles were 77, and 51 nm on using graphite and MPC-150, respectively (Fig. 3a–f, S2 and S3†). Moreover, the significantly wider distribution of particle size of NbC on graphite than MPC-150 implies the presence of spatially limited area on MPC-150.

In this context, NbC was synthesized with MPCs which possess pore sizes of 30 nm (MPC-30) and 10 nm (MPC-10) to investigate the effect of the pore. The XRD measurement revealed the D values of NbC synthesized with MPC-30 (D = 30 nm) or MPC-10 (D = 27 nm), indicating that crystalline sizes were not dependent on the pore sizes of MPCs (Fig. S4†). On the other hand, TEM observation clearly revealed that the size of NbC nanoparticles synthesized with MPC-30, in which average particle size was 30 nm, decreased compared to that prepared with MPC-150 (Fig. 3g, h, k and S5†). Notably, the average particle size of NbC obtained from MPC-10 (average size: 29 nm) was almost identical to the condition under the usage of MPC-30, and the size was larger than their pore size (Fig. 3i, j, l and S6†). This finding indicates that the reaction does not proceed in the mesopore but at the external surface. To visualize the reaction field, scanning electron microscopy (SEM) was performed (Fig. 4). Intriguingly, few NbC particle exists in the pore of MPC, demonstrating the formation of NbC occurs at the external surface of MPC. The origin of differences in particle size on the used MPC was considered by the calculation of the external surfaces area (S^{ext}) for each MPC from Brunauer–Emmett–Teller surface area (S^{BET}) and the internal surface area of the pore (S^{int}) estimated by N_2 adsorption/desorption experiments: $S^{ext} = S^{BET} - S^{int}$ (Fig. S7,† and Table 1). The S^{ext} for the MPC-150, MPC-30, and MPC-10 were 26.0, 49.9, and 32.3 $m^2 g^{-1}$, respectively. The slight difference in S^{ext} compared to S^{BET} indicates that the MPC with smaller pores possesses a larger number of pores per weight. In such a situation, the area of a limited external surface encompassed by mesopores as a reaction field became smaller. Hence, the smaller particle sizes were afforded in the case of MPC with small pores.

The impact of calcination temperatures on the formation of NbC was also investigated. Fig. 5 shows XRD patterns of the products after calcination at different temperatures (800–1000 °C). NbC could be successfully synthesized alone above 1000 °C (see Fig. 2 for the calcination at 1150 °C), while potassium niobate ($KNbO_3$) was observable at 900 °C, and other potassium niobate species ($K_4Nb_6O_{17}$) was also detected in addition to $KNbO_3$ in the case of calcination at 800 °C. However, $KNbO_3$ completely deteriorated and only diffraction peaks arising from

NbC appeared on the calcination at 900 °C for 20 h (Fig. S8†). Weakening peaks of $K_4Nb_6O_{17}$ and $KNbO_3$ accompanied with strengthen of the NbC peak was also observed by calcination at 800 °C for 40 h, too (Fig. S8†). Notably, no NbC was generated on the calcination at 900 °C at 20 h in the absence of K_2CO_3 (Fig. S9†), therefore the niobates were reaction-active species. Since $K_4Nb_6O_{17}$ is an intermediate in the formation of $KNbO_3$ from Nb_2O_5 and K_2CO_3,[33,34] these findings indicate that NbC is formed by the reaction of carbon and $KNbO_3$. Here, the intermediated $KNbO_3$ is expected to have an extraordinary

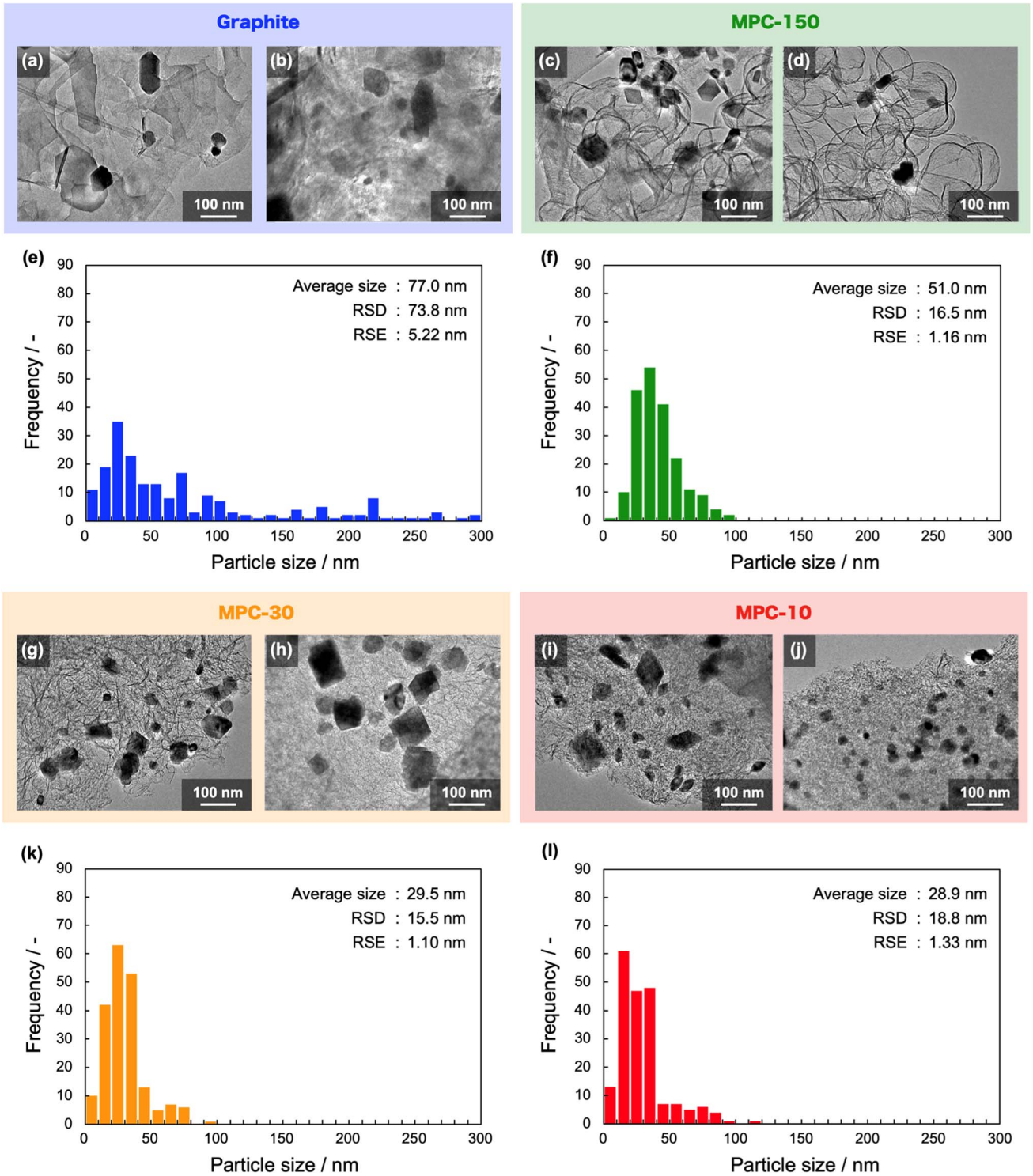

Fig. 3 (a–d and g–j) TEM images of synthesized NbC particles with (a and b) graphite, (c and d) MPC-150, (g and h) MPC-30, and (i and j) MPC-10 as carbon sources. (e, f, k and l) size distributions of the NbC nanoparticles synthesized with (e) graphite, (f) MPC-150, (k) MPC-30, and (l) MPC-10. The distribution was estimated by the measuring particle sizes of NbC in TEM images. The terms RSD and RSE indicate "relative standard deviation" and "relative standard error", respectively.

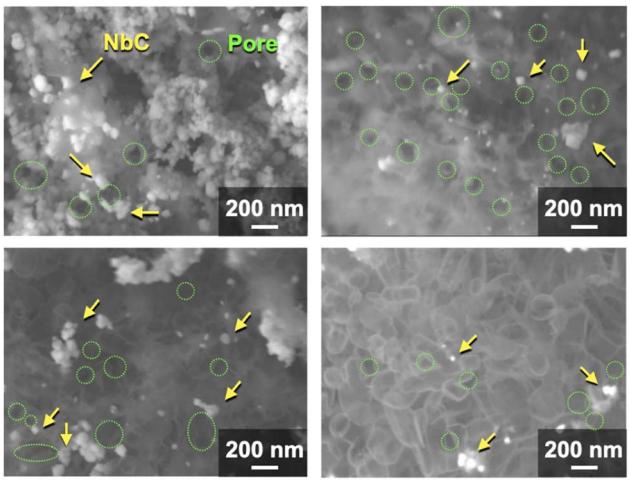

Fig. 4 SEM images of synthesized NbC by the calcination of the mixture of Nb_2O_5 (0.1 g) MPC-150 (0.1 g), and K_2CO_3 (0.035 g) at 1150 °C for 10 under N_2 stream atmosphere.

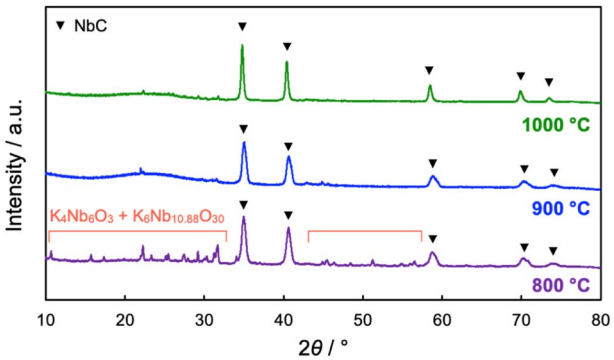

Fig. 5 XRD patterns of products after calcination of the mixture of Nb_2O_5 (0.1 g) MPC-150 (0.1 g), and K_2CO_3 (0.035 g) at different temperatures for 10 h under N_2 stream atmosphere. The yields of NbC were estimated to be 60.8, 85.5, and 85.5% on the calcination at 800, 900, 1000 °C, respectively.

contribution to selective reaction at the external surface of MPC. Capillary action (CA) is generally the dominant driving force on incursion of liquid into the nano-scale pores and its magnitude is strongly dependent on the affinity between the liquid and substrate possessing pores.[35] Since ionic $KNbO_3$ molten, composed of K^+ and $[NbO_6]^{7-}$ octahedra,[36,37] disfavors hydrophobic MPC, the CA is not preferred, resulting in the prohibition of the incursion of $KNbO_3$ molten into the pore of MPC. The D values of NbC became smaller as the calcination temperature decreased, *i.e.* $D = 36$, 31, and 17 nm for 1150 °C (10 h), 1000 °C (10 h), and 900 °C (20 h), respectively. The average particle sizes of NbC estimated from TEM observation also coincided with this tendency (Fig. S10 and S11†). The decrease in the particle sizes was due to preventing sintering, and particle sizes of NbC could be changed in our novel alkali-molten synthetic method with MPC by the variation calcination temperature.

Table 1 Brunauer–Emmett–Teller surface areas (S^{BET}), internal surface areas arising from mesopores (S^{int}) estimated by Barrett–Joyner–Halenda (BJH) method, and external surface area (S^{ext}) of MPC-150, MPC-30, and MPC-10. S^{ext} was calculated by the equation as follow: $S^{ext} = S^{BET} - S^{int}$

Type of MPC	$S^{BET}/m^2\ g^{-1}$	$S^{int}/m^2\ g^{-1}$	$S^{ext}/m^2\ g^{-1}$
MPC-150	203.2	177.2	26.0
MPC-30	695.0	645.1	49.9
MPC-10	1055.9	1023.6	32.3

According to the result mentioned above, Nb_2O_5 stepwise changed to NbC *via* $KNbO_3$ intermediate. To clarify the reaction mechanism on the first step, from Nb_2O_5 to $KNbO_3$, thermogravimetry (TG) was performed for Nb_2O_5, K_2CO_3, and the mixture of Nb_2O_5 and K_2CO_3 (Fig. 6). Weight was identical on the elevation of temperature in the case of Nb_2O_5, while the clear weight loss from 50 °C to 175 °C of temperature range was observable on the K_2CO_3 and their mixture. The decrease in the weight is attributed to the dehydration of K_2CO_3.[38] In addition to the dehydration, second 1.13 mg of weight loss could be seen in only the mixture. A gaseous by-product was responsible for the weight loss since $KNbO_3$ was never evaporated at 900 °C, hence mass spectrometry of possible gaseous products during temperature elevation was performed for the mixture of Nb_2O_5 and K_2CO_3 (Fig. S12†). The mass signals strongly indicate that only CO_2 ($m/z = 44$) was produced as gaseous products, which is reasonable because the theoretical stoichiometric amount of emitted CO_2 in the reaction was 1.02 mg, coinciding with the experimental value (1.13 mg). Thus, the first step in the synthesis of NbC can be described as eqn (1), which is well-matched with the result mentioned in the effect of calcination temperature.

$$Nb_2O_5 + K_2CO_3 \rightarrow 2KNbO_3 + CO_2 \quad (1)$$

Here, K_2CO_3 used in this experiment (2.53×10^{-4} mol) was stoichiometrically lacking to Nb_2O_5 (3.76×10^{-4} mol), but a complete transformation of Nb_2O_5 to $KNbO_3$ could be explained by the discussion mentioned below.

The reaction mechanism in the second step was hence tracked by using commercial $KNbO_3$ and MPC-150. The XRD measurement strongly suggests that $KNbO_3$ is the reactant for the formation of NbC (Fig. S13†). The weight of the mixture of $KNbO_3$ and MPC-150 decreased by 92.0 mg after calcination. Here, K_2O is known to be degraded to K_2O_2 and K above 360 °C.[39] The K_2O_2 again afford K_2CO_3 by reacting with CO,[39] while K evaporates above 757 °C.[40] Hence, not only the gaseous materials but also K_2O can be the product responsible for weight loss. If the CO_2 was formed in this process under estimation of evaporation of K_2O, the theoretical weight loss was 76.9 mg, while the weight loss was 88.1 mg in the case of the formation of CO. Hence, CO is preferred as the product because of well matching the experimental data. Therefore, a possible reaction can be depicted as follow.

$$2KNbO_3 + 7C \rightarrow 2NbC + 5CO + K_2O \quad (2)$$

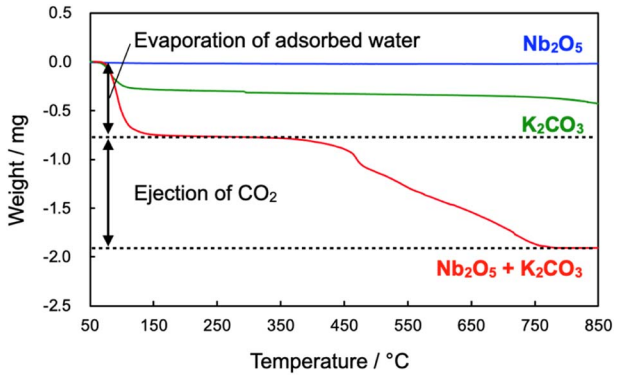

Fig. 6 TG profiles of Nb_2O_5, K_2CO_3 and their mixture during temperature elevation at the rate of 10 °C min^{-1} under N_2 atmosphere.

It should be noted that K_2O likely to reacts with Nb_2O_5 in the case of the existence of Nb_2O_5.[41] Indeed, the reaction of Nb_2O_5 and KOH at 700 °C afforded $KNbO_3$ (Fig. S14†), where reaction temperature was set to 700 °C to laten carbonization of $KNbO_3$ and KOH transformed into K_2O by dehydration at this temperature.[42] The reaction of K_2O with Nb_2O_5 well explains the fact that no Nb_2O_5 remains despite the condition of the stoichiometric lacking of K_2CO_3 to Nb_2O_5 for all experiments. Hence the following equation can be described.

$$Nb_2O_5 + K_2O \rightarrow 2KNbO_3 \quad (3)$$

The entire reaction mechanism was proposed from the findings of experiments. On the direct reaction at the first step, Nb_2O_5 was transformed into $KNbO_3$ by the reaction with K_2CO_3 (eqn (1)) and K_2O was generated as a by-product. The K_2O further makes Nb_2O_5 change $KNbO_3$ (eqn (3)) or reacts with CO_2 to regenerate K_2CO_3 (ref. 43) (eqn (4)). On the other hand, since NbO_2 was also formed in the absence of K_2CO_3 (Fig. 2), indirect paths from NbO_2 should be also considered (eqn (5)–(7)). The second step is the carbonization of intermediated $KNbO_3$ on the external surface of MPC (eqn (2)). The selective proceeding at the external surface is due to the inhibition of CA as mentioned above. All considerable elemental reactions in the synthesis of NbC nanoparticles using MPC are shown as follows.

First step

(Direct reaction from Nb_2O_5)

$$Nb_2O_5 + K_2CO_3 \rightarrow 2KNbO_3 + CO_2 \quad (1)$$

$$Nb_2O_5 + K_2O \rightarrow 2KNbO_3 \quad (3)$$

$$K_2O + CO_2 \rightarrow K_2CO_3 \quad (4)$$

(Indirect reaction *via* NbO_2)

$$Nb_2O_5 + C \rightarrow 2NbO_2 + CO \quad (5)$$

$$Nb_2O_5 + CO \rightarrow 2NbO_2 + CO_2 \quad (6)$$

$$2NbO_2 + K_2CO_3 \rightarrow 2KNbO_3 + CO \quad (7)$$

Second step

$$2KNbO_3 + 7C \rightarrow 2NbC + 5CO + K_2O \quad (2)$$

Experimental

Synthesis of niobium(IV) carbide (NbC)

0.1 g of graphite (8.33×10^{-3} mol, KANTO CHEMICAL Co., Inc.) or MPC (8.33×10^{-3} mol, TOYO TANSO Co., Ltd), 0.1 g of Nb_2O_5 (3.76×10^{-4} mol, FUJIFILM Wako Pure Chemical Co., Ltd), and 0.035 g of K_2CO_3 (2.53×10^{-4} mol, FUJIFILM Wako Pure Chemical Co., Ltd) were mixed by mortar and obtained mixture was added on the platinum boat. The reactants on the platinum boat were placed in the oven and calcined at different temperature (800–1150 °C) for 10 h under N_2 atmosphere. After cooling to room temperature, NbC was obtained. On the investigation of reaction mechanism, $KNbO_3$ (KOJUNDO CHEMICAL LABORATORY Co., Ltd) was also used as reactants.

X-ray diffraction (XRD) measurement

The XRD analysis was performed using Ultima-IV apparatus (Rigaku Co., Ltd). All samples were irradiated with Cu Kα (λ = 0.154 nm) at a voltage of 40 kV and current of 40 mA. The scanning range and scanning speed were set to 5°–80° and 2.0° min^{-1} for all the measurements. The "D/teX Ultra" was utilized as a detector. A crystalline size (D) was calculated by Scherrer equation as shown below:

$$D = \frac{K\lambda}{\beta \cos \theta} \quad (8)$$

where, K, β, and θ represent shape factor, dull widths at half maximum, and diffraction angle, respectively. The composition of the resulting materials was simply quantified by using reference intensity ratio (RIR) method.

Nitrogen (N_2) adsorption/desorption test

N_2 adsorption/desorption isotherms were recorded by a BELSORP-mini II apparatus (MicrotracBEL Co., Ltd). 10 mg of sample was placed in a glass cell and was heated at 150 °C for 2 h *in vacuo* as pre-treatment. N_2 adsorption experiments were performed at −196 °C.

Thermogravimetry (TG)

Thermogravimetry-differential thermal analyzer (Thermo plus EVO, Rigaku Co., Ltd) was used for TG-DTA, and the sample was added into a platinum pan (SHIMADZU). The α-alumina was used as a reference. On the investigation of mechanism, the sample was heated from 25 to 900 °C at the rate of 10 °C min^{-1} under N_2 stream condition.

Temperature-programed mass spectrometry

The mixture of Nb_2O_5 (0.1 g) and K_2CO_3 (0.035 g) in the glass cell was heated to 1000 °C at the rate of 5.0 °C min^{-1} by using BELCAT II apparatus (MicrotracBEL Co., Ltd). The ejected

gaseous component was analyzed by mass spectrometry using BELMASS (MicrotracBEL Co., Ltd).

Transmission electron microscopy (TEM)

All samples were added in ethanol and the suspensions were sonicated. The suspensions were dip on the Cu microgrid (Okenshoji Co., Ltd) and dried. TEM images were observed at 200 kV using a JEM-2100F (JEOL) system.

Scanning electron microscopy (SEM)

The resulting NbC was placed onto carbon tape equipped with alumina substrate (Okenshoji Co., Ltd) and SEM images of it were observed by field-emission scanning electron microscopy (FE-SEM, JSM-7400F, JEOL) with a measurement condition as follow: 5 kV of voltage, 1.0×10^{-10} A of current, and 8 mm of working distance.

Conclusions

We succeeded in the fabrication of NbC nanoparticles with a size of 30–50 nm by a novel alkali-molten salt method using MPCs. The NbC nanoparticles became smaller when MPC possessing small pore size was used due to the decreasing in area of the external surface encompassed by pores as reaction field. The particle sizes of NbC were also changeable by calcination temperature. Furthermore, all considerable elemental reactions were demonstrated by the X-ray spectroscopic, thermogravimetric, and mass spectrometric analyses. We believe that the strategy in the present study has an extraordinary contribution to the field of material chemistry and accelerates development of nano-sized functional materials.

Author contributions

Keigo Tashiro: preparation of manuscript, TEM observation, analyses. Shogo Kobayashi: preparation of manuscript, experiments, analyses. Hinako Inoue: experiments. Shuhei Shimoda: preparation of manuscript, TEM observation. Akihide Yanagita: TEM observation. Shigeo Satokawa: preparation of manuscript.

Conflicts of interest

There are no conflicts to declare.

Acknowledgements

This study was supported by the Joint Usage/Research Center for Catalysis, Hokkaido University.

References

1 C. B. Peres, P. M. R. Resende, L. J. R. Nunes and L. C. de Marais, *Clean Technol.*, 2022, **4**, 1193–1207.
2 M. González-Castaño, B. Dorneanu and H. Arellano-García, *React. Chem. Eng.*, 2021, **6**, 954–976.
3 X. Pan, F. Jiao, D. Miao and X. Bao, *Chem. Rev.*, 2021, **121**, 6588–6609.
4 S. Sun, H. Sun, P. T. Williams and C. Wu, *Sustainable Energy Fuels*, 2021, **5**, 4546–4559.
5 A. J. Barrios, D. V. Peron, A. Chakkingal, A. I. Dugulan, S. Moldovan, K. Nakouri, J. Thuriot-Roukos, R. Wojcieszak, J. W. Thybaut, M. Virginie and A. Y. Khodakov, *ACS Catal.*, 2022, **12**, 3211–3225.
6 C. Giornado and M. Antonietti, *Nano Today*, 2011, **6**, 366–380.
7 J. G. Chen, *Chem. Rev.*, 1996, **96**, 1477–1498.
8 D. J. Ham and J. S. Lee, *Energies*, 2009, **2**, 873–899.
9 D. Zeng and M. J. Hampden-Smith, *Chem. Mater.*, 1992, **4**, 968–970.
10 Y. Xiao, J.-Y. Hwang and Y.-K. Sun, *J. Mater. Chem. A*, 2016, **4**, 10379–10393.
11 H. Zhang, X. Yang, H. Zhang, J. Ma, Z. Huang, J. Li and Y. Wang, *Chem. - Eur. J.*, 2021, **27**, 5074–5090.
12 H. Prats, J. J. Piñero, F. Viñes, S. T. Bromley, R. Sayós and F. Illas, *Chem. Commun.*, 2019, **55**, 12797–12800.
13 S. Meyer, A. V. Nikiforov, I. M. Petrushina, K. Köhler, E. Christensen, J. O. Jensen and N. J. Bjerrum, *Int. J. Hydrogen Energy*, 2015, **40**, 2905–2911.
14 T. Wakisaka, K. Kusada, D. Wu, T. Yamamoto, T. Toriyama, S. Matsumura, H. Akiba, O. Yamamuro, K. Ikeda, T. Otomo, N. Palina, Y. Chen, L. S. R. Kumara, C. Song, O. Sakata, W. Xie, M. Koyama, Y. Kubota, S. Kawaguchi, R. L. Arevalo, S. M. Aspera, E. F. Arguelles, H. Nakanishi and H. Kitagawa, *J. Am. Chem. Soc.*, 2020, **142**, 1247–1253.
15 S. Ahmad, I. Ashraf, M. A. Mansoor, S. Rizwan and M. Iqbal, *Nanomaterials*, 2021, **11**, 776.
16 H. Zhang, J. Liu, Z. Tian, Y. Ye, Y. Cai, C. Liang and K. Terabe, *Carbon*, 2016, **100**, 590–599.
17 C. Kunkel, F. Viñes and F. Illas, *Energy Environ. Sci.*, 2016, **9**, 141–144.
18 K.-H. Wu, Y. Jiang, S. Jiao, K.-C. Chou and G.-H. Zhang, *J. Mater. Res. Technol.*, 2020, **9**, 11778–11790.
19 Y. Lian, N. Yang, D. Wang, Y. Zheng, C. Ban, J. Zhao and H. Zhang, *Adv. Energy Sustainability Res.*, 2020, **1**, 2000038.
20 V. L. S. T. da Silva, M. Schmal and S. T. Oyama, *J. Solid State Chem.*, 1996, **123**, 168–182.
21 B. Deng, Z. Wang, W. Chen, j. T. Li, D. X. Luong, R. A. Carter, G. Gao, B. I. Yakobson, Y. Zhao and J. M. Tour, *Nat. Commun.*, 2022, **13**, 262.
22 N. S. Alhajri, D. H. Anjum, M. N. Hedhili and K. Takanabe, *ChemistrySelect*, 2016, **2**, 290–296.
23 S. Qin, B. Liao, L. Mao and F. Xiao, *Mater. Lett.*, 2014, **121**, 162–165.
24 R. Mahle, P. L. Mahapatra, A. K. Singh, P. Kumbhakar, M. Paliwal, C. S. Tiwary and R. Banerjee, *ACS Sustainable Chem. Eng.*, 2022, **10**, 13650–13660.
25 A. Gupta, M. Mittal, M. K. Singh, S. L. Suib and O. P. Pandey, *Sci. Rep.*, 2018, **8**, 13597.
26 L. Yate, L. E. Coy, G. Wang, M. Baltrán, E. Díaz-Barriga, E. M. Saucedo, M. A. Ceniceros, K. Załęski, I. Llarena, M. Möller and R. F. Ziolo, *RSC Adv.*, 2014, **4**, 61355–61362.
27 M. Lei, H. Zhao, H. Yang, B. Song and W. H. Tang, *J. Eur. Ceram. Soc.*, 2008, **28**, 1671–1677.

28 D. E. Grove, U. Gupta and A. W. Castleman Jr, *Langmuir*, 2010, **26**, 16517–16521.
29 P. G. Li, M. Lei, Z. B. Sun, L. Z. Cao, Y. F. Guo, X. Guo and W. H. Tang, *J. Alloys Compd.*, 2007, **430**, 237–240.
30 E. Coy, Y. Yate, D. P. Valencia, W. Aperador, K. Siuzdak, P. Torruella, E. Azanza, S. Estrade, I. Iatsunskyi, F. Peiro, X. Zhang, J. Tejada and R. F. Ziolo, *ACS Appl. Mater. Interfaces*, 2017, **9**, 30872–30879.
31 J. Ma, M. Wu, Y. Du, S. Chen, W. Jin, L. Fu, Q. Yang and A. Wen, *J. Alloys Compd.*, 2009, **475**, 415–417.
32 Y. Du, M. Lei, H. Yang and X. Wang, *J. Wuhan Univ. Technol., Mater. Sci. Ed.*, 2008, **23**, 779–782.
33 S. Uchida, Y. Inoue, Y. Fujishiro and T. Sato, *J. Mater. Sci.*, 1998, **33**, 5125–5129.
34 D.-H. Kim, M.-R. Joung, I.-T. Seo, J. Hur, J.-H. Kim, B.-Y. Kim, H.-J. Lee and S. Nahm, *J. Eur. Ceram. Soc.*, 2014, **34**, 4193–4200.
35 A. Depalo and A. C. Santomaso, *Colloids Surf., A*, 2013, **436**, 371–379.
36 A. I. Stash, E. O. Terekhova, S. A. Ivanov and V. G. Tsirelson, *Acta Crystallogr., Sect. B: Struct. Sci., Cryst. Eng. Mater.*, 2021, **77**, 728–739.
37 D. Yang, Y. Wang, L. Li, M. Yao, W. Zhang, H. Gu, S. Zhang, M. Fan, G. A. Sewvandi and D. Hu, *Inorg. Chem.*, 2021, **60**, 97–107.
38 N. Mazur, H. Huinink, B. Borm, S. Sansota, H. Fischer and O. Adan, *Thermochim. Acta*, 2022, **715**, 179286.
39 J. M. Illingworth, B. Rand and P. T. Williams, *Fuel Process. Technol.*, 2022, **235**, 107348.
40 F. Aitken and F. Volino, *Phys. Fluids*, 2022, **34**, 017112.
41 X. Hong, L. Lu, Y. Zhao and X. Wu, *Chin. Phys. Lett.*, 1995, **12**, 83–86.
42 H. M. Yang, D. H. Zhang, Y. Chen, M. J. Ran and J. C. Gu, *Earth Environ. Sci.*, 2017, **69**, 012051.
43 S. Yokoyama, K. Tanaka, M. Seisho and H. Haneda, *J. Jpn. Pet. Inst.*, 1983, **26**, 462–466.